

This is the accepted manuscript made available via CHORUS. The article has been published as:

Structure and energetics of interlayer dislocations in bilayer graphene

Shuyang Dai, Yang Xiang, and David J. Srolovitz

Phys. Rev. B **93**, 085410 — Published 8 February 2016

DOI: [10.1103/PhysRevB.93.085410](https://doi.org/10.1103/PhysRevB.93.085410)

Structure and energetics of interlayer dislocations in bilayer graphene

Shuyang Dai¹, Yang Xiang², and David J. Srolovitz^{1,3}

¹*Department of Materials Science and Engineering,*

University of Pennsylvania, Philadelphia, Pennsylvania 19104, USA

²*Department of Mathematics, Hong Kong University of Science and Technology, Hong Kong, China*

³*Department of Mechanical Engineering and Applied Mechanics,*

University of Pennsylvania, Philadelphia, Pennsylvania 19104, USA

(Dated: January 19, 2016)

We present a general hybrid model based upon the continuum generalized Peierls-Nabarro model (with density functional theory parametrization) to describe interlayer dislocations in bilayer systems. In this model, the bilayer system is divided into two linear elastic 2D sheets, the strains in each sheet can be relaxed by both elastic in-plane deformation and out-of-plane buckling; this deformation is described via classical linear elastic thin plate theory. The interlayer bonding between these two sheets is described by a 3-dimensional Generalized Stacking-Fault Energy (GSFE) determined from first principle calculations and based upon the relative displacement between the sheets. The structure and energetics of various interlayer dislocations in bilayer graphene was determined by minimizing the elastic and bonding energy with respect to all displacements. The dislocations break into partials and pronounced buckling is observed at the partial dislocation locations to relax the strain induced by their edge components. The partial dislocation core width is reduced by buckling. An analytical model is also developed based upon the results obtained in numerical simulation. We develop an analytical model for the bilayer structure and energy and show that these predictions are in excellent agreement with the numerical results.

PACS numbers: 68.65.Pq, 68.55.-a, 62.20.mq

I. INTRODUCTION

Since the successful exfoliation of monolayer graphene, its extraordinary physical properties have been widely investigated and show promise for future nanotechnology applications¹. Recently, bilayer graphene, the stacked counterpart of monolayer graphene, has attracted increasing attention, in part, because its bandgap is tunable up to 300 meV¹. Bandgap modulation induced by application of an electric field in bilayer graphene has been experimentally confirmed². The bandgap of layered materials, such as bilayer graphene³⁻⁵, hexagonal boron nitride, MoS₂ as well as phosphorene can also be varied by changes in bilayer stacking³⁻⁸ and elastic strain⁸⁻¹⁰.

While the relatively weak vdW-like interactions between graphene layers (compared to the strong interlayer covalent bonds) are sufficient to adhere two layers, the energy difference and barriers between different (sliding) translational states are sufficiently small that several distinct bilayer states can be realized. Mechanical procedures used to assemble bilayer graphene inevitably lead to a variety of translation states, often in a single graphene bilayer. Dislocation lines, lying between the two graphene sheets that compose the bilayer, separate domains in the bilayer that are in different translational states. Grain boundaries between two layers that are rotated with respect to one another (i.e., twist boundaries) can be described as arrays of dislocations plus stacking faults (metastable translation states). The Generalized Stacking-Fault Energy¹¹ (GSFE, i.e., the energy landscape associated with uniformly translating one layer with respect to the other) can be used to understand (and predict) both dislocation and bilayer twist bound-

ary structure and properties.

In two-dimensional materials, such as monolayer graphene, the term dislocation is usually used to describe point like (0D) defects lying within the sheet; e.g., pentagon-heptagon or square-octagon pairs. Such defects are edge dislocations with line directions oriented normal to the sheet. Unlike in monolayers, in bilayers it is also possible to have one-dimensional (line) dislocations. Such linear defects are interlayer dislocations that lie between the two layers of a bilayer material - these dislocations do not require the generation of any topological defects within either sheet to form. Also, unlike in monolayers, where the motion of point-like dislocations require a large energy ~ 7 eV¹² (because of the covalent nature of the bonding), we expect that the weak van der Waals bonding between graphene layers should lead to very small activation energies for the glide of such 1D interlayer dislocations in bilayer graphene.

A general model for describing dislocations and twist boundaries in bilayer systems can be derived on the basis of earlier models for dislocations in three-dimensional materials and thin films. For example, an edge dislocation in a free-standing thin film will bend the film through an angle $\theta = 3b/2h$, where b is the magnitude of the Burgers vector and h is the film thickness¹³. This demonstrates that the elastic field of a dislocation can bend/buckle free standing films. The applicability of this result to bilayer graphene is not straightforward because it is both extremely elastically anisotropic and sliding between layers can occur. The latter can lead to different translational states on each side of the dislocation; i.e., dislocations in graphene can break into partial dislocations. An appropriate model must account for both of

these effects.

Recently, buckling has been observed in bilayer graphene and investigated via TEM, diffraction and atomistic simulation¹⁴. Butz *et al.*¹⁴ showed that the amplitude of the buckling in bilayer graphene is ~ 1 nm and the width of the buckled region is several tens of nanometers. Compared with a flat bilayer, buckling substantially reduces the dislocation core width and relaxes the dislocation line energy in a free standing bilayer. Another recent study analyzed interlayer dislocations in bilayer graphene on the basis of a one-dimensional, Frenkel-Kontorova-like model¹⁵, in which a dislocation is treated as a soliton. While interesting and reasonable, such an idealized model predicts dislocation core widths significantly larger than experimentally observed¹⁵.

In this paper, we present a general approach based upon a Peierls-Nabarro model to describe interlayer dislocations in bilayer materials. In the classical Peierls-Nabarro model^{16–18} (and its generalizations^{19,20}), the material is divided into two semi-infinite linear elastic continua by the dislocation slip plane, the interface between these two continua have a relative displacement (disregistry) in the presence of dislocations, and the two continua are connected via a nonlinear function (atomic bonding) of the disregistry. We adopt a similar approach, replacing the semi-infinite crystal continua with 2D membranes. The strains in the membranes relax in-plane elastic deformation and out-of-plane buckling; the membrane deformation is described via linear elastic thin plate theory^{21–23}. The GSFE describes the bonding between graphene sheets. The structure and deformation of the bilayer with a dislocation is determined by the force balance between the local stresses in the graphene sheets and the restoring force from the interlayer bonding, as represented by the GSFE. We apply this approach to determine the structure and energetics of four interlayer dislocations in bilayer graphene: edge, screw, 30° , and 60° (i.e., the angles between the Burgers vector and the line direction). We determine the buckling amplitude, in-plane strain distributions, partial dislocation structures, core widths and dislocation energies. Based on these results, we construct a simple analytical model to describe the buckling and in-plane deformation of bilayer graphene with dislocations of arbitrary Burgers vector and show that the analytical model is in excellent agreement with the simulation results.

II. HYBRID MODEL FOR BILAYER STRUCTURE

Figure 1(a) shows 2D views of the bilayer with an interlayer dislocation. First, the natural state consists of two flat, parallel elastic sheets without any deformation. In the x_1 direction, the lengths of the upper and lower layers are l_{1+}^0 and l_{1-}^0 (Fig. 1(a1)). Next, we uniformly compress/stretch the upper/lower layer to the same length l_1^0 such that there is no net stress in the bilayer (Fig. 1(a2)).

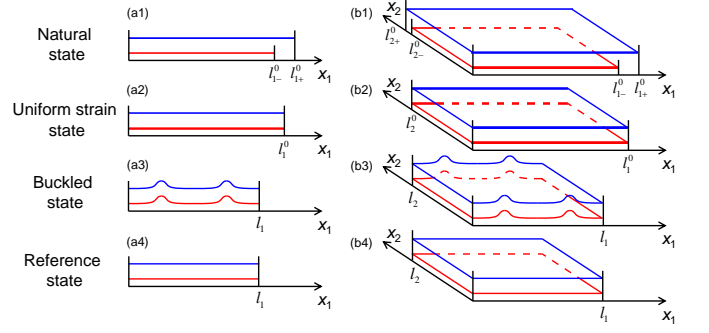


FIG. 1. Schematic illustrations of the bilayer system with (a) 2D and (b) 3D views, indicating [(a1) and (b1)] its natural state; [(a2) and (b2)] its uniformly strained state; [(a3) and (b3)] its buckled state; and [(a4) and (b4)] its reference state. The Burgers vector is $\mathbf{b} = (l_{1+}^0 - l_{1-}^0)\hat{x}_1$.

The “buckled state” is found by minimizing the system energy (Fig. 1(a3)). Its projected length is l_1 ($l_1 < l_1^0$ due to buckling); we also introduce a flat “reference state” of the same length (Fig. 1(a4)). There are uniform normal strains $\varepsilon_{ii\pm}^0 = (l_i - l_{i\pm}^0)/l_{i\pm}^0$ ($i = 1, 2$) in the reference state (Fig. 1(b4)), $\varepsilon_{ii+}^0 = (l_{i-}^0/l_{i+}^0)\varepsilon_{ii-}^0 - (l_{i+}^0 - l_{i-}^0)/l_{i+}^0$, where $i \in \{1, 2\}$.

The total energy of the bilayer consists of the elastic energy E_e and the misfit energy E_m (the bonding energy between the two layers); i.e.,

$$E_t = E_{e+} + E_{e-} + E_m, \quad (1)$$

where $+/-$ represents the upper/lower layers.

The elastic energy of a single layer $E_{e\pm}$ has contributions from in-plane strains $E_{s\pm}$ and bending $E_{b\pm}$ ^{21,23,24} ($E_{e\pm} = E_{s\pm} + E_{b\pm}$):

$$E_{s\pm} = \frac{1}{2} \int \varepsilon_{\pm}^T \mathbf{C}_{\pm} \varepsilon_{\pm} dx_1 dx_2, \quad (2)$$

$$E_{b\pm} = \frac{1}{2} \int \kappa_{\pm} H_{\pm}^2 dx_1 dx_2, \quad (3)$$

where ε_{\pm} are the in-plane strain tensors, \mathbf{C}_{\pm} are the anisotropic elastic constant tensors, κ_{\pm} are bending rigidities corresponding to the mean curvature H_{\pm} . The strains in the buckled layer need to include the effects of deflection away from the flat configuration,

$$\varepsilon_{\pm} = \varepsilon_{\pm}^0 + (\nabla \mathbf{u}_{\pm} + \nabla \mathbf{u}_{\pm}^T + \nabla f_{\pm} \otimes \nabla f_{\pm})/2, \quad (4)$$

where $\mathbf{u}_{\pm} = (u_{1\pm}, u_{2\pm})$ are the x_1, x_2 displacement vectors and ε_{\pm}^0 are the reference strains. The mean curvature of each layer is calculated from its vertical (z) displacement f_{\pm} .²¹

The misfit energy E_m associated with the vdW interactions between the layers is

$$E_m = \int \Gamma(\mathbf{u}^{\perp}, f^{\perp}) dx_1 dx_2, \quad (5)$$

where $\Gamma(\mathbf{u}^\perp, f^\perp)$ is the 3D GSFE^{5,11}, and $\mathbf{u}^\perp = (u_1^\perp, u_2^\perp)$ is the relative in-plane displacement between the layers (measured in the deformed configuration), and f^\perp is the interlayer separation (measured along the layer normal). The relative displacements between the two buckled layers are $u_i^\perp = (\varepsilon_{ii+}^0 - \varepsilon_{ii-}^0)x_i + (u_{i+} - u_{i-}) + \frac{1}{2}(\frac{\partial f_+}{\partial x_i} + \frac{\partial f_-}{\partial x_i})(d_0 + f_+ - f_-)$ and $f^\perp = f_+ - f_- + d_0$. In the results presented below, we use the 3D GSFE reported by Zhou, et al.⁵.

The equilibrium bilayer structure can be obtained by minimizing the total energy with respect to the six functions, $u_{1\pm}(x_1, x_2)$, $u_{2\pm}(x_1, x_2)$, and $f_\pm(x_1, x_2)$. The equilibrium equations for those variables are

$$\frac{\delta E_t}{\delta u_{i\pm}} = -C_{ijkl\pm} \frac{\partial \varepsilon_{kl}}{\partial x_j} \pm \frac{\partial \Gamma}{\partial u_i^\perp} = 0, \quad (6)$$

$$\begin{aligned} \frac{\delta E_t}{\delta f_\pm} = & -C_{ijkl\pm} \frac{\partial}{\partial x_i} \left(\varepsilon_{kl} \frac{\partial f_\pm}{\partial x_j} \right) + \kappa \Delta^2 f_\pm \pm \frac{\partial \Gamma}{\partial u_i^\perp} \frac{\partial f_\mp}{\partial x_i} \\ & \pm \frac{\partial \Gamma}{\partial f^\perp} - \frac{1}{2} \frac{\partial^2 \Gamma}{\partial u_i^\perp \partial u_j^\perp} \frac{\partial u_j^\perp}{\partial x_i} (f_+ - f_-) = 0. \end{aligned} \quad (7)$$

The minimum energy configuration can be found by iterating the following set of equations to convergence:

$$\frac{\partial u_{i\pm}}{\partial t} = -\frac{\delta E_t}{\delta u_{i\pm}}, \quad \frac{\partial f_\pm}{\partial t} = -\frac{\delta E_t}{\delta f_\pm}. \quad (8)$$

These equations are solved using the fast Fourier transform method with a semi-implicit scheme, i.e., the linear (non-linear) terms are discretized using an implicit (explicit) scheme. The numerical details are in the Supplemental Material (SM).

III. INTERLAYER DISLOCATION-INDUCED BUCKLING

We apply the model to describe the buckling of bilayer graphene in the presence of interlayer dislocations. We assume that the dislocation is straight and lies along the x_2 -axis; the edge and screw components of the Burgers vector of the dislocation are $b_e = \mathbf{b} \cdot \hat{x}_1$ and $b_s = \mathbf{b} \cdot \hat{x}_2$, respectively. For the case of a straight dislocation, all of the displacements and strains are uniform along x_2 ; hence, there is only one variable x_1 in all of the simulations. The edge component b_e can be thought of as originating from the addition of an extra atomic period in the x_1 -direction; this is the origin of the length differences of the two layers along x_1 contributes to the natural state in Fig. 1; i.e., $l_{1+}^0 = l_{1-}^0 - b_e$. The screw components of the Burgers vector do not induce any natural length differences between the two layers, i.e., $l_{2+}^0 = l_{2-}^0$.

In this paper, we consider four types of dislocations (i.e., with different orientations of the Burgers vector with respect to the line direction, θ): (1) edge 90° ($b_e = -a_0$, $b_s = 0$); (2) mixed 60° ($b_e = -\sqrt{3}a_0/2$, $b_s = -a_0/2$), (3) mixed 30° ($b_e = -a_0/2$, $b_s = \sqrt{3}a_0/2$),

and (4) screw 0° ($b_e = 0$, $b_s = -a_0$), where $a_0 = 0.242$ nm is the carbon-carbon separation along the zigzag direction. For the edge and mixed 30° dislocations, the x_1 and x_2 axes are along the $[11\bar{2}0]$ and $[\bar{1}100]$ directions, respectively, and for the mixed 60° and screw dislocation, the x_1 and x_2 axes are along the $[\bar{1}100]$ and $[11\bar{2}0]$ directions. It is well known that basal dislocations in graphite can dissociate into pairs of partial dislocations, separated by a planar stacking-fault²⁵ with a finite stacking fault energy (per area). In bilayer graphene, the same type of dissociation occurs¹⁴; see Table I. Upon crossing from one side of a partial dislocation to the other, the local stacking order changes from AB to AC. These two stacking sequences are equivalent in bilayer graphene (not so in graphite) and, hence, there is no energy difference between these (i.e., the stacking fault energy in bilayer graphene is exactly zero)^{5,14}.

TABLE I. Partial dissociation in bilayer graphene.

Dislocation	\mathbf{b}^a	Partial A		Partial B	
		\mathbf{b}_A^b	θ^c	\mathbf{b}_B	θ
Edge 90°	$a_0[\bar{1}\bar{1}20]/3$	$a_0[\bar{1}010]/3$	60°	$a_0[0\bar{1}10]/3$	120°
Mixed 60°	$a_0[\bar{2}110]/3$	$a_0[\bar{1}100]/3$	90°	$a_0[\bar{1}010]/3$	150°
Mixed 30°	$a_0[\bar{2}110]/3$	$a_0[\bar{1}010]/3$	60°	$a_0[\bar{1}100]/3$	0°
Screw 0°	$a_0[\bar{1}\bar{1}20]/3$	$a_0[0\bar{1}10]/3$	150°	$a_0[\bar{1}010]/3$	150°

^a \mathbf{b} is the Burgers vector of the full dislocation.

^b \mathbf{b}_A and \mathbf{b}_B are the Burgers vectors of partial dislocations A and B, respectively.

^c θ is the angle between the Burgers vector and the dislocation line direction.

In our simulations, the only input into the hybrid model is the elastic properties of each monolayer (based on AIREBO²⁶ potential calculations²³ - $C_{11} = 312.67$ J/m², $C_{12} = 91.66$ J/m², $C_{44} = 110.40$ J/m², and $\kappa = 22.08 \times 10^{-20}$ J) and the interlayer 3D GSFE. The 3D GSFE employed here was determined by fitting to accurate density functional theory results obtained using the adiabatic-connection fluctuation-dissipation theorem within the random phase approximation²⁷⁻²⁹ (ACFDT-RPA) by Zhou et al.⁵.

A. Edge dislocation

Figure 2 shows the main edge dislocation results. In the buckled state, the bilayer projection length (see Fig. 1(a3)) is $l_1 = 72.52$ nm. The edge dislocation decomposes into two partials and buckles upward by ~ 1.4 nm. Note that the amplitude of the buckling is almost identical in the upper and lower layers. The slope of the bilayer profile (Fig. 2(b)) shows a sawtooth-like form, with two abrupt jumps at the positions of the partial dislocations. Figure 2(c) shows that the curvature of each layer is nearly constant except very near the partial dislocation cores where it is approximately Gaussian. The width of the Gaussian provides a good measure of the

dislocation core size; we measure the FWHM core size from this to be ~ 2.4 nm.

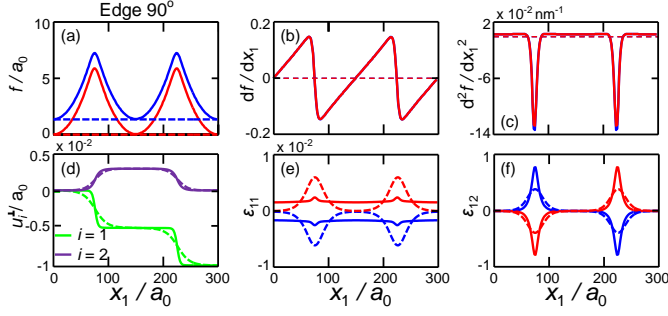


FIG. 2. The first two panels are the variation of the layer (a) profiles f , (b) gradient of the profiles df/dx_1 , (c) the mean curvature of the layers, (d) the relative displacements between two layers u^\perp , strains (e) ε_{11} and (f) ε_{12} as a function of distance x_1 along the bilayer. The blue and red solid curves correspond to the upper and lower layers, and the solid and dashed curves to the buckled and flat bilayer cases, respectively. The third panel is the layer profiles f for (g) Mixed 60° , (h) Mixed 30° , and (i) Screw 0° dislocations.

Figure 2(d) shows the relative displacements along the x_1 and x_2 direction, u_1^\perp and u_2^\perp (corresponding to the edge and screw components of the Burgers vector). These displacement profiles are approximately piecewise constant (each constant region corresponds to perfect AB/AC stacking of the bilayer) with jumps in between these. The jump magnitudes are $(-a_0/2, a_0/2\sqrt{3})$ and $(-a_0/2, -a_0/2\sqrt{3})$. These two components correspond to the edge and screw components of the partial dislocation Burgers vectors. The dislocation core widths, deduced from these data, are nearly the same width as estimated from Fig. 2(c).

The in-plane strains ε_{11} and ε_{12} for each layer are shown in Fig 2(e) and (f). In both cases, the strains are nearly zero except in the vicinity of the dislocation cores. ε_{11} shows peaks of the same sign in each layer, while ε_{12} shows peaks with opposite signs in each layer. This corresponds to the sign of the edge and screw components of the two partials, i.e., $b_{A,e} = b_{B,e} = -a_0/2$ and $b_{A,s} = -b_{B,s} = a_0/2\sqrt{3}$. Unlike in bulk materials, here, the amplitude of the strain ε_{11} is much smaller than the strain ε_{12} ; we return to this below.

In order to clarify the effects of layer buckling, we also consider the case where the bilayer is flat $f_\pm = 0$; see the dashed lines in Fig. 2. Trivially, the profile of f versus x_1 and all its derivatives are zero in this case (Fig. 2(a)-(c)). However, comparison of the results in Fig. 2(d)-(f) between the buckled and flat geometries is instructive. The partial dislocation core widths for the case where the layers are flat can be estimated from Figs. 2(d)-(f). We measure the core widths to be ~ 6.3 nm which is larger than in the buckled case by a factor of ~ 2.5 .

The total energy has contributions from in-plane strain, bending and misfit, as shown in Table III and the corresponding profiles shown in Fig. 3. Focusing first on the

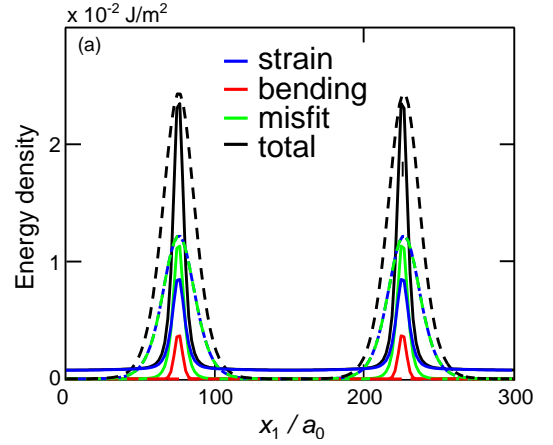


FIG. 3. The total and component energy densities of the buckled (solid lines) and flat (dashed lines) graphene bilayers containing an edge dislocation.

buckled case, we see that the in-plane strain energy is larger than the misfit and much larger than the bending energy (these energies are the integrals under the curves in Fig. 3). The energy density peak heights for the bending and strain are nearly equal to the misfit energy. This demonstrates that very little energy is stored in the bending degree of freedom of the bilayer. For the flat case, the in-plane strain energy (since there is no bending here, this energy is the entire elastic energy) and the misfit energy are almost perfectly balanced. Comparison of the buckled and flat cases show that buckling decreases the dislocation energy by nearly a factor of two. The energy density curves show that peak heights for the total energy and misfit energy are almost identical in the two cases. The difference in energy is attributable to the fact that buckling decreases the dislocation core width (Fig. 3).

TABLE II. Core width for different partial dislocations (nm).

	Edge 90°	Mixed 60°	Mixed 30°	Screw 0°
Buckled (Flat)	1.5 (7.2)	2.4 (6.3)	3.7 (5.3)	4.5 (4.5)

We also compare our bilayer graphene simulation results to those obtained from the fully atomistic simulations of Butz et al.¹⁴, as shown in Fig. 4 (we interpolate the discrete atomistic data, as discussed in the Supplementary Material).³⁰ In the atomistic simulations¹⁴, the empirical AIREBO potential²⁶ and a registry-dependent interlayer potential³¹ were used to describe the in-plane carbon bonds and interlayer interactions in bilayer graphene, respectively. Butz et al.¹⁴ implemented these potentials^{26,31} within the molecular dynamics simulation package LAMMPS³². Examination of this figure and the more detailed Fig. S1 in the SM show that our continuum-based model provides an excellent quantitative match to the atomistic simulation results and validates our continuum-based model. The very small deviations are likely the result of two factors. First,

the atomistic simulations are based on an empirical interatomic potential (the registry-dependent interlayer potential was fit to density functional theory results in the local density approximation) while our continuum-based model was parameterized from accurate first principles (GSFE) data (obtained using the more reliable ACFDT-RPA approach⁵) and elastic constants. The second is due to the differences of relaxation methods and convergence criteria (the energy differences involved are extremely small, hence exact coincidence between our model and the atomistic simulations is not expected). The overall excellent agreement suggests that model is quantitative.

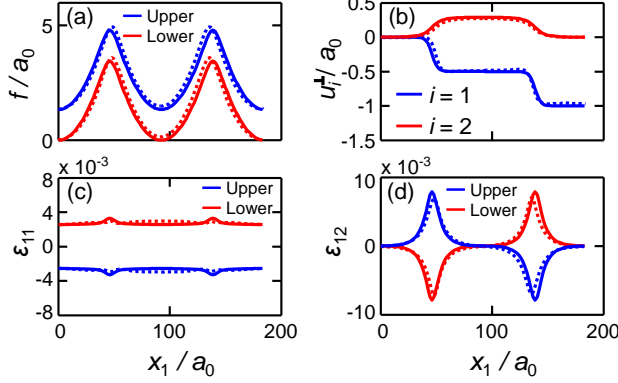


FIG. 4. Comparison between the results from this study and the atomistic results from Butz *et al.*¹⁴. The solid and dashed curves represent the model and atomistic results, respectively. Panel (a) represents the vertical displacement f , (b) relative displacements between the layers, and the strain (c) ϵ_{11} and (d) ϵ_{12} profiles. An enlarged view of (a) can be found in the Supplementary Material along with the un-interpolated atomistic simulation data.

B. Simulation results for other dislocations

In this section, we show the results for other three types of interlayer dislocations: (1) mixed 60° ($b_e = -\sqrt{3}a_0/2$, $b_s = -a_0/2$), (2) mixed 30° ($b_e = -a_0/2$, $b_s = \sqrt{3}a_0/2$), and (3) screw 0° ($b_e = 0$, $b_s = -a_0$). For the mixed 30° dislocations, the x_1 and x_2 axes are along the $[11\bar{2}0]$ and $[\bar{1}100]$ directions, respectively, and for the mixed 60° and screw dislocation, the x_1 and x_2 axes are along the $[1\bar{1}00]$ and $[11\bar{2}0]$ directions.

The edge dislocation results demonstrate that the dislocation dissociates into a pair of 60° partial dislocations that are identical (apart from a mirror symmetry; AB/AC vs. AC/AB). We demonstrate here that other dislocations also dissociate into partials but these partials are, in general, inequivalent (the exceptions are the pure edge and pure screw cases). In Fig. 5, we show the model results for the 60° , 30° , and pure screw dislocations, as shown for the edge dislocation in Fig. 2.

The 60° dislocation (Fig. 5(a)) decomposes into edge and 30° partials. The amplitude of the profile and the

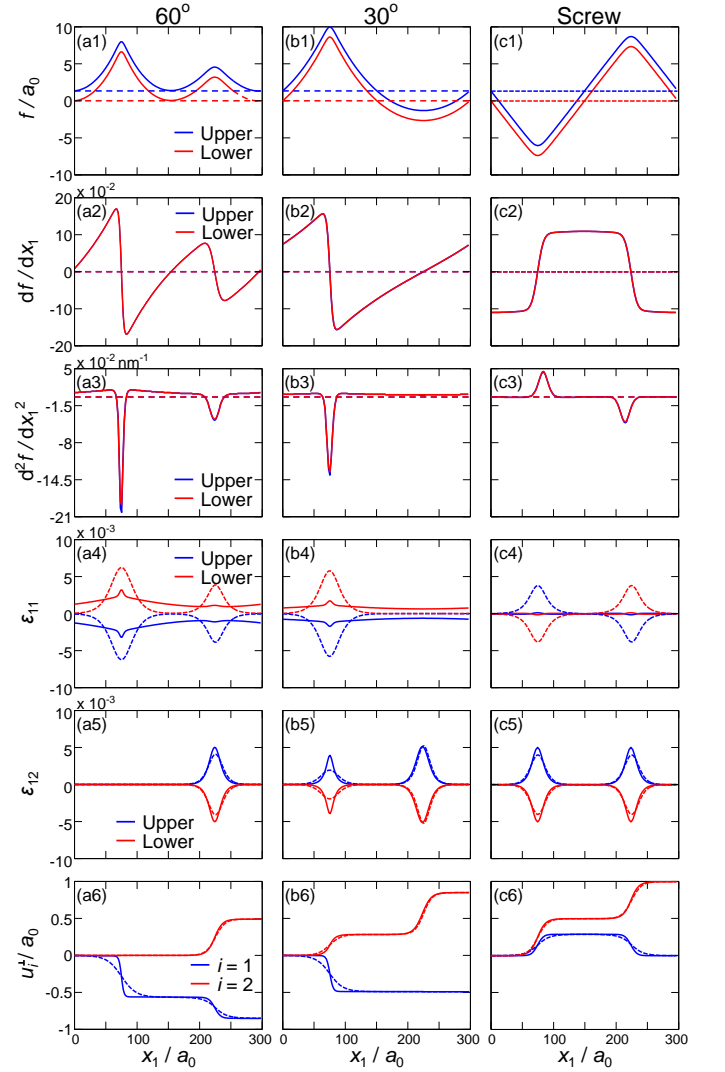


FIG. 5. Results for general dislocations in buckled configuration (Solid lines) and flat configuration (Dashed lines). Left column: Mixed 30° dislocation; Middle column: Mixed 60° dislocation; Right column: Screw dislocation.

jump in df/dx_1 at the edge partial is larger than that of the 30° partial. The jump in df/dx_1 at the dislocation core tells us the turning angle of the profile f there. Figure 5(a4) shows the ϵ_{11} profile and also shows that this strain associated with the edge partial is larger than that associated with the 30° partial; this is because this strain component is related to the edge component of the Burgers vector. On the other hand, the strain that couples to the screw component of the Burgers vector ϵ_{12} (Fig. 5(a5)) does show the edge partial. The 30° partial also appears in this profile because it has mixed edge/screw character. Finally, the displacement difference profile (Fig. 5(a6)) shows either just the edge partial or both partials, depending upon whether the displacement component is parallel or perpendicular to the dislocation line direction.

A mixed 30° dislocation dissociates into a 60° partial and a screw (0°) partial. Surprisingly, examination of Fig. 5(b1) shows only the 60° partial (the other partial is present, but not visible). Comparison with Fig. 2(a) shows that this partial is identical with the 60° partial seen in the pure edge case. The missing partial is pure screw. This suggests that the edge component of the partial dislocation Burgers vector controls sharp bending; no edge component implies no sharp bend. The curvature between the partial and next image (across the periodic boundary condition) is nearly constant (Figs. 5(b1)-(b3)). Figure 5(b4) shows no hints of the second partial; this is because this partial has no edge component. The profile of ε_{12} (Fig. 5(b5)) does show this screw partial. Examination of Figs. 5(a) and (b) show that the turning angle increases in magnitude from the screw partial to the 30° partial to the 60° partial to the edge partial (Fig. 5(a)). This is, in fact, the order in which the edge component of the Burgers vector increases.

As noted above, the bilayer curvature is uniform between the edge partial and its periodic image, (i.e., the slope of d^2f/dx_1^2 vs. x_1 is constant). However, more care examination of Figs. 5(b2) and (b3) demonstrate that this is only approximately true. We believe that this is a numerical convergence issue; since the bending energy is so small, achieving very uniform curvature would require a more severe convergence criteria than we are able to achieve within our numerical method (also see Figs. 5(a2) and (a3)).

Figure 5(c) shows that a screw dislocation dissociates into two 30° partials. The structures of these partials are identical to that of the 30° partial found upon the dissociation of the 60° dislocation case, Fig. 5(b). Unlike the layer profiles found for the other dislocations (edge, 30° and 60° dislocations), each of the layers here is flat, except for in the immediate vicinity of the dislocation cores. At the dislocation cores, the bilayer profile bends on a small length scale, resulting in a sawtooth bilayer profile. This observation is also confirmed by Fig. 5(c2) where we see that df/dx_1 is approximately piecewise constant.

We now examine the question of how the out-of-plane buckling affects the dislocation core size. This can be deduced from Figs. 2 and 5, where we plot the results for the flat (dashed curves) and buckled bilayers, and from Table II. As we saw in the previous section in the discussion of the edge dislocation case, buckling leads to a large reduction in partial dislocation core width. We observe exactly the same result for the partials of the non-screw dislocations. However, examination of Fig. 5(b5) and Table III shows that this is only true for non-screw partials; i.e., the dislocation core for the screw partial is exactly the same width in the flat and buckled cases. Table III further demonstrates that the magnitude of the reduction of the core width on going from flat to buckled increases as the edge character of the partial increases.

The core width is determined by a competition between the misfit energy (favoring perfect AB/AC reg-

TABLE III. Contributions to the energy (per unit length) for the edge dislocation (10^{-10} J/m). The values in the brackets are for the flat case. All energies refer to the entire bilayer. θ is the angle between the Burgers vector and the dislocation line direction.

θ	l_{1-}^0	Buckled (Flat)			
		E_s	E_b	E_m	E_t
90°	$200a_0$	1.30 (1.65)	0.13 (0.00)	0.53 (1.61)	1.97 (3.26)
	$300a_0$	1.00 (1.63)	0.14 (0.00)	0.53 (1.63)	1.67 (3.26)
	$400a_0$	0.85 (1.63)	0.14 (0.00)	0.53 (1.63)	1.52 (3.26)
60°	$200a_0$	1.16(1.54)	0.13 (0.00)	0.60(1.52)	1.89(3.06)
	$300a_0$	0.96(1.53)	0.13(0.00)	0.61(1.53)	1.69(3.06)
	$400a_0$	0.86(1.53)	0.13(0.00)	0.61(1.53)	1.60(3.06)
30°	$200a_0$	0.95(1.35)	0.069(0.00)	0.79(1.35)	1.81(2.69)
	$300a_0$	0.88(1.35)	0.07(0.00)	0.79(1.35)	1.74(2.69)
	$400a_0$	0.85(1.35)	0.07(0.00)	0.79(1.35)	1.71(2.69)
0°	$200a_0$	0.88(1.26)	0.03(0.00)	0.91(1.26)	1.81(2.51)
	$300a_0$	0.88(1.26)	0.03(0.00)	0.91(1.26)	1.81(2.51)
	$400a_0$	0.88(1.26)	0.03(0.00)	0.91(1.26)	1.81(2.51)

istry) and the elastic energy (favoring uniform strains). In bulk materials (and the flat case), large in-plane elastic stiffness and small resistance to shear between the layers leads to large dislocation core widths¹⁶. However, when the bilayer is not constrained to be flat, the normal strain (ε_{11}) is almost completely relaxed by buckling - leading to a significant decrease in E_s . This reduces the elastic contribution in this competition and, hence, leads to a significant reduction in the core width relative to the flat case (where ε_{11} is large). As b_e decreases, the magnitude of E_s relaxed by buckling is smaller and of course the core width reduction is also smaller. We note that while buckling efficiently reduces ε_{11} , associated with the edge component of the Burgers vector, it cannot reduce ε_{12} , associated with the screw component. In fact, the peak height in ε_{12} is even larger when buckling occurs, compared with the flat case. This is simply the result of the smaller core size in the buckled case.

IV. ANALYTICAL MODEL FOR BILAYER DISLOCATION

The results can be used as a guide to develop a simplified model for the structure of bilayer graphene and determine the interactions between dislocations in bilayer graphene.

We first observe that the profiles of f_+ and f_- are nearly identical (other than a shift) for all of the dislocations studied. We also note that these dislocations always dissociate into partials. It is reasonable to treat these bilayers as consisting of two distinct regions. The first is the dislocation core region, where there is a rapid variation of all of the structural properties with respect

to x_1 . df_{\pm}/dx_1 show a (relatively) abrupt jump and the magnitude of the jump is proportional to the edge component of the Burgers vector of the partial dislocation, i.e., the edge partial has the largest jump, the screw partial has the smallest (none) and the jump of the mixed partials lies in between. The width of this region (1.6 nm to 4.5 nm) is very narrow compared with the simulation cell size or the spacing between partial dislocations. The second region is between the partials, which is quite wide compared with the core size. In this region, df_{\pm}/dx_1 has (nearly) constant slope, which implies that the layer curvature is nearly constant and the bilayer shape between the partials is nearly parabolic. Moreover, in this region, the structural properties, including the relative displacements u_1^{\perp} and u_2^{\perp} , the strains $\varepsilon_{11\pm}$ and $\varepsilon_{12\pm}$, and the energy density, are nearly independent of position x_1 and $\varepsilon_{11+} = -\varepsilon_{11-}$, $\varepsilon_{12+} = \varepsilon_{12-}$, and $d^2f_+/dx_1^2 = d^2f_-/dx_1^2$. This implies that the elastic energy here is nearly constant and the misfit energy $E_m \approx 0$.

Based upon these observations, we construct an analytical model for dislocations in bilayers, in which the core width is assumed to be zero such that the gradient of f_+ and f_- and the relative displacements u_1^{\perp} and u_2^{\perp} have discontinuous jumps at the position of the dislocation. The magnitude of the jump in f at the cores is related to the edge component of the partial dislocation and should be b_e/d_0 , where b_e is the edge component of the partial. The magnitude of the jump in u_1^{\perp} (u_2^{\perp}) at the cores is equal to the edge (screw) component of the partial dislocation. The slopes of df_{\pm}/dx_1 and the profiles of u_1^{\perp} and u_2^{\perp} in the inter-partial region are constants. We further assume $f = f_+ = f_-$. In our analytical model, the two partials are separated by a distance d_D ; the partials are at $x_1 = (l - d_D)/2$ and $x_1 = (l + d_D)/2$. Therefore the structure and the energy of the bilayer system can be obtained from the df/dx_1 , u_1^{\perp} and u_2^{\perp} profiles. See the SM for more details. The total energy of the bilayer system with interlayer dislocations has contributions from the core and elastic energy (the first is localized in the core region and the second is associated with the curved regions between the partials), i.e.,

$$E = E_{\text{edge}}(\sin^2 \theta_A + \sin^2 \theta_B) + E_{\text{screw}}(\cos^2 \theta_A + \cos^2 \theta_B) + \frac{C_{11}(b_{A,e} + b_{B,e})^2}{4l} + \frac{\kappa(b_{A,e} + b_{B,e})^2}{ld_0^2}. \quad (9)$$

By fitting Eq. (9) to the simulation results shown in Table III, the core energy for pure edge and pure screw partial dislocations can be obtained: $E_{\text{edge}} = 0.318 \times 10^{-10}$ and $E_{\text{screw}} = 1.091 \times 10^{-10}$ J/m. The model discussed above suggests that the total energy of a dislocation in bilayer graphene can be determined solely in terms of the elastic constants, total Burgers vector, bending rigidity and the partial dislocation core energy (as determined from the simulation results above). Figure 6 shows a comparison of the analytical expression for the total energy of the dislocation (per unit length) Eq. (9) with the results from the simulations for bilayer graphene.

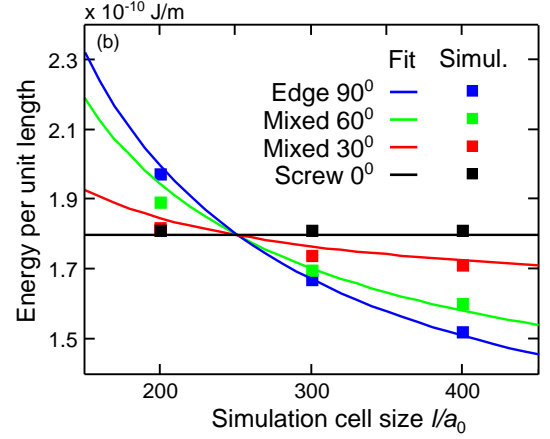


FIG. 6. Plot of the comparisons of E_t based on the multiscale simulation results and the proposed analytical form (Eq. (9)) for four different types of dislocations with two fitting parameters E_{edge} and E_{screw} .

Clearly, the agreement between theory and simulation is good with no fitting parameters other than the pure edge and screw core energies. This, together with the comparisons between the predicting bilayer profiles (see the SM) and the comparison with atomistic simulation results (Fig. 4) demonstrates the validity of the simulation results and the analytical model.

Note that in an infinite bilayer, Eq. (9) shows that the force between dislocations is zero (i.e., E_{total} is independent of d_D). This is a direct result of the assumption that the dislocation core is of zero width. This assumption implies that there will be no interactions between dislocation cores and that the inter-partial dislocation regions have profiles determined solely by the elastic properties of the layers and the boundary conditions imposed by the core. Clearly, the simulations show that this is not quite true and the dislocation cores do have (a small, but) finite width. When the dislocations are well separated, the effect of finite core width is very small and can normally be ignored. This does, however, lead to a small dependence on simulation cell size (spacing between partial dislocations in our system), as shown in Table III. The force between two dislocations arising from this small core effect can be understood by consideration of simple models such as the Frenkel-Kontorova model or sine-Gordon equation³³. These models suggest that the cores are soliton-like and the core-core interaction energy decays exponentially with dislocation separation d_D .

Compared to the forces between dislocations in bulk crystalline materials, where forces between dislocations decay inversely with separation, such interactions between dislocations in bilayer graphene material are extremely small. Also, unlike bulk crystalline materials where the energy of a dislocation diverges as the sample size tends to infinity, in bilayer graphene, the dislocation energy is always finite.

V. DISCUSSION AND CONCLUSIONS

We have presented a continuum-based model for general dislocations in bilayer systems which are free to buckle or constrained to remain flat. Our approach is based upon the Peierls-Nabarro model, generalized to account for the thin sheet elasticity of vdW layers and an accurate description of the interaction between graphene layers. It explicitly considers both the in-plane and out-of-plane deformation of the layer in addition to a 3D GSFE for the interactions between layers. The results show that dislocations in graphene bilayers decompose into partial dislocations and that the bilayer will buckle with a magnitude that depends on the edge component of the partial dislocation. This out-of-plane deformation is critical for the determination of the structure and energetics of dislocations in bilayer graphene, as well as such properties as partial dislocation core width. The simulation results were validated by comparison with the atomistic simulation results¹⁴.

The input for the model only requires the 3D GSFE and the elastic constants for individual layers. Hence, this model can be directly applied to any vdW bilayer system (such as BN/BN) in addition to bilayer graphene. Further, the model is also directly applicable to hetero-bilayer systems (such as graphene/boron nitride) where misfit dislocations are always present (because of mismatches in the lattice parameters of the two sheets). Such mismatch implies the presence of an array of dislocations with edge character. This model can also be extended to the case of twisted bilayer structure, i.e., the two layers are rotated with respect to one another. Such a twist interface/boundary necessarily leads to a

Moiré structure³⁴. However, the experimentally observed twist boundaries have structures unlike the rigid twist Moiré patterns¹⁵; rather the pattern is strongly influenced by the types of local relaxation considered here (for small twist angles such structures are periodic networks of predominantly screw dislocations that break into a partial dislocation array). For twist boundaries in hetero-bilayers, this predominantly screw dislocation network will be superimposed on the edge dislocation network described above.

Based on the continuum-based model results presented here, we constructed a simple analytical model for dislocations in bilayers. We demonstrated that this model accurately reproduces the simulation results for all dislocations with only two parameters to be determined from simulation. This model shows that, to first order, dislocations in vdW bilayers do not interact with each other. However, when two dislocations are very close, there will be an exponentially decaying force associated with core-core interactions.

ACKNOWLEDGMENTS

We thank Prof. Bernd Meyer for providing the data files containing his atomistic simulation results. The work of S.D. and D.J.S. was supported as part of the Center for the Computational Design of Functional Layered Materials, an Energy Frontier Research Center funded by the U.S. Department of Energy (DOE), Office of Science, Basic Energy Sciences (BES) under Award # DE-SC0012575. The work of Y.X. was partially supported by the Hong Kong Research Grants Council General Research Fund 606313.

-
- ¹ A. K. Geim and K. S. Novoselov, *Nat. Mater.* **6**, 183 (2007).
 - ² Y. Zhang, T.-T. Tang, C. Girit, Z. Hao, M. C. Martin, A. Zettl, M. F. Crommie, Y. R. Shen, and F. Wang, *Nature* **459**, 820 (2009).
 - ³ A. A. Avetisyan, B. Partoens, and F. M. Peeters, *Phys. Rev. B* **81**, 115432 (2010).
 - ⁴ A. Agar, E. J. H. Lee, K. Balasubramanian, M. Burghard, and K. Kern, *Nano Lett.* **9**, 3124 (2009).
 - ⁵ S. Zhou, J. Han, S. Dai, J. Sun, and D. J. Srolovitz, *Phys. Rev. B* **92**, 155438 (2015).
 - ⁶ N. Marom, J. Bernstein, J. Garel, A. Tkatchenko, E. Joselevich, L. Kronik, and O. Hod, *Phys. Rev. Lett.* **105**, 046801 (2010).
 - ⁷ J. Dai and X. C. Zeng, *J. Phys. Chem. Lett.* **5**, 1289 (2014).
 - ⁸ M. Wu, X. Qian, and J. Li, *Nano Lett.* **14**, 5350 (2014).
 - ⁹ J.-H. Wong, B.-R. Wu, and M.-F. Lin, *J. Phys. Chem. C* **116**, 8271 (2012).
 - ¹⁰ H. J. Conley, B. Wang, J. I. Ziegler, J. Richard F. Haglund, S. T. Pantelides, and K. I. Bolotin, *Nano Lett.* **13**, 3626 (2013).
 - ¹¹ V. Vitek, *Philos. Mag.* **18**, 773 (1968).
 - ¹² C. Gong, A. W. Robertson, K. He, G.-D. Lee, E. Yoon, C. S. Allen, A. I. Kirkland, and J. H. Warner, *ASC Nano* **9(10)**, 10066 (2015).
 - ¹³ R. Siems, P. Delavignette, and S. Amelinckx, *Physica Status Solidi (b)* **2**, 421 (1962).
 - ¹⁴ B. Butz, C. Dolle, F. N. D. Weber, D. Waldmann, H. B. Weber, B. Meyer, and E. Spiecker, *Nature* **505**, 533 (2014).
 - ¹⁵ J. S. Alden, A. W. Tsen, P. Y. Huang, R. Hovden, L. Brown, J. Park, D. A. Muller, and P. L. McEuen, *PNAS* **110**, 11256 (2013).
 - ¹⁶ J. P. Hirth and J. Lothe, *Theory of Dislocations*, 2nd ed. (John Wiley, New York, 1982).
 - ¹⁷ R. Peierls, *Proc. Phys. Soc.* **52**, 34 (1940).
 - ¹⁸ F. R. N. Nabarro, *Proc. Phys. Soc.* **59**, 256 (1947).
 - ¹⁹ Y. Xiang, H. Wei, P. Ming, and W. E, *Acta Mater.* **56**, 1447 (2008).
 - ²⁰ S. Dai, Y. Xiang, and D. J. Srolovitz, *Acta Mater.* **61**, 1327 (2013).
 - ²¹ L. D. Landau and E. M. Lifshitz, *Theory of Elasticity* (Butterworth-Heinemann, 1986).
 - ²² S. Kumar, K. P. S. S. Hembram, and U. V. Waghmare, *Phys. Rev. B* **82**, 115411 (2010).
 - ²³ S. Chen and D. C. Chrzan, *Phys. Rev. B* **84**, 214103 (2011).

- ²⁴ S. A. Safran, *Statistical Thermodynamics of surfaces, Interfaces and Membranes* (Addison-Wesley Publishing Company, 1994).
- ²⁵ P. Delavignette and S. Amelinckx, *J. Nucl. Mater.* **5**, 17 (1962).
- ²⁶ D. W. Brenner, O. A. Shenderova, J. A. Harrison, S. J. Stuart, B. Ni, and S. B. Sinnott, *J. Phys. Condens. Matter* **14**, 783 (2002).
- ²⁷ J. Harl and G. Kresse, *Phys. Rev. B* **77**, 045136 (2008).
- ²⁸ J. Harl and G. Kresse, *Phys. Rev. Lett.* **103**, 056401 (2009).
- ²⁹ J. Harl, L. Schimka, and G. Kresse, *Phys. Rev. B* **81**, 115126 (2010).
- ³⁰ The Atomic coordinates of all of the carbon atoms in the bi-layer graphene data reported in Butz et al.¹⁴ was provided by Bernd Meyer (one of its co-authors).
- ³¹ A. N. Kolmogorov and V. H. Crespi, *Phys. Rev. B* **71**, 235415 (2005).
- ³² S. Plimpton, *J. Comp. Phys* **117**, 1 (1995).
- ³³ Y. Hsu, *Phys. Rev. D* **22**, 1394 (1980).
- ³⁴ Z. Y. Rong and P. Kuiper, *Phys. Rev. B* **48**, 17427 (1993).